Am J Physiol Heart Circ Physiol 295: H898–H906, 2008.
First published May 30, 2008; doi:10.1152/ajpheart.00309.2008.

Three-dimensional localization and quantification of PAF-induced gap formation in intact venular microvessels

Yanyan Jiang,[1]* Ke Wen,[1,2]* Xueping Zhou,[1]* Diane Schwegler-Berry,[3] Vince Castranova,[3] and Pingnian He[1]

[1]*Department of Physiology and Pharmacology, West Virginia University, Morgantown, West Virginia;* [2]*Department of Pharmacology, Tianjin Medical University, Tianjin, China; and* [3]*Pathology and Physiology Research Branch, Health Effects Laboratory Division, National Institute for Occupational Safety and Health, Morgantown, West Virginia*

Submitted 23 March 2008; accepted in final form 27 May 2008

Jiang Y, Wen K, Zhou X, Schwegler-Berry D, Castranova V, He P. Three-dimensional localization and quantification of PAF-induced gap formation in intact venular microvessels. *Am J Physiol Heart Circ Physiol* 295: H898–H906, 2008. First published May 30, 2008; doi:10.1152/ajpheart.00309.2008.—Combining single-vessel perfusion technique with confocal microscopy, this study presents a new approach that allows three-dimensional visualization and quantification of endothelial gaps under experimental conditions identical to those used to measure permeability coefficients, endothelial calcium concentration, and nitric oxide production in individually perfused intact microvessels. This approach provides an efficient means for defining the transport pathways and cellular mechanisms of increased microvascular permeability during inflammation. Platelet-activating factor (PAF) was used to increase the permeability of individually perfused rat mesenteric venules. Fluorescent microspheres (FMs, 100 nm) were used as leakage markers, and confocal images were acquired at successive focal planes through the perfused microvessel. Perfusion of FMs under control conditions produced a thin, uniform layer of FMs in the vessel lumen, but in PAF-stimulated microvessels significant amounts of FMs accumulated at endothelial junctions. Reconstructed confocal images three-dimensionally delineated the temporal and spatial development of endothelial gaps in PAF-stimulated microvessels. The FM accumulation, quantified as the total fluorescence intensity per square micrometer of vessel wall, was 8.4 ± 1.8 times the control value within 10 min of PAF perfusion and declined to 5.0 ± 0.6 and 1.4 ± 0.2 times the control value when FMs were applied 30 and 60 min after PAF perfusion. The changes in the magnitude of FM accumulation closely correlated with the time course of PAF-induced increases in hydraulic conductivity (L_p), indicating that the opening and closing of endothelial gaps contributed to the transient increase in L_p in PAF-stimulated microvessels. Electron microscopic evaluations confirmed PAF-induced gap formation and FM accumulation at endothelial clefts.

hydraulic conductivity; microvessel permeability; fluorescent microspheres; confocal microscopy; endothelial gap formation

INCREASES IN VASCULAR PERMEABILITY occur in a variety of cardiovascular diseases and are implicated in tissue edema and organ dysfunction. Comprehensive assessments of the exchange functions of the vascular wall are critical for defining the cellular and molecular mechanisms responsible for permeability increases and disease progression. Microvascular exchange has often been assessed by measuring hydraulic conductivity (L_p) or the solute permeability coefficient, which are quantitative measures of the mean fluxes from a segment of the vessel driven by differences in pressure and solute concentration across the vascular wall (32). However, increases in vascular permeability are usually heterogeneous, and gap formation at endothelial junctions has been recognized as the main pathway leading to increased permeability (8, 9, 28). For over a decade, endothelial gaps have been mainly described either by two-dimensional localization of leakage sites via systemic injection of markers or by electron microscopic findings from very limited vessel regions (2, 23, 28, 33). There are currently no approaches available that allow a three-dimensional assessment of endothelial gap formation in intact microvessels.

The objective of this study was to develop a method that allows three-dimensional visualization and quantification of formed endothelial gaps under experimental conditions identical to those used to measure permeability coefficients, endothelial cytoplasmic calcium concentration ($[Ca^{2+}]_i$), and nitric oxide (NO) production, thus providing an efficient means for defining the transport pathways and cellular mechanisms responsible for increased permeability in intact microvessels under inflammatory conditions. Fluorescent microspheres (FMs) were used as leakage markers, and stacks of confocal images were acquired from individually perfused rat mesenteric venular microvessels in the presence or absence of an inflammatory stimulus. The reconstructed images provided a three-dimensional view of FM accumulation of intact vascular walls. Experiments were designed to characterize platelet-activating factor (PAF)-induced FM accumulation and to evaluate whether the magnitude of FM accumulation enables it to serve as a measure of the magnitude of the endothelial gaps formed in a perfused vessel segment. We also aimed to conduct a quantitative comparison between the extent of formed endothelial gaps and the magnitude of L_p increases in PAF-stimulated microvessels. To define the cellular changes and FM location at an ultrastructural level, electron microscopy studies were performed on vessels prepared with experimental procedures identical to those used for confocal imaging and L_p measurements. To demonstrate the potential applications of this method, we also investigated the effect of 8-bromo-cAMP (8-BrcAMP), an agent that prevents inflammatory mediator-induced permeability increases (19, 20), on PAF-induced gap formation.

* Y. Jiang, K. Wen, and X. Zhou made equal contributions to this manuscript.

Address for reprint requests and other correspondence: P. He, Dept. of Physiology and Pharmacology, School of Medicine, West Virginia Univ., Morgantown, WV 26506-9229 (e-mail: phe@hsc.wvu.edu).

The costs of publication of this article were defrayed in part by the payment of page charges. The article must therefore be hereby marked "*advertisement*" in accordance with 18 U.S.C. Section 1734 solely to indicate this fact.

MATERIALS AND METHODS

Animal preparation. Experiments were carried out on female Sprague-Dawley rats (2–3 mo old, 220–250 g; Hilltop Laboratory Animals, Scottdale, PA) anesthetized with pentobarbital sodium (65 mg/kg body wt) given subcutaneously. Additional 3-mg doses were given as needed to maintain anesthesia during the experiment. All procedures and animal usage were approved by the Animal Care and Use Committee at West Virginia University. Each rat was anesthetized, the trachea was intubated, and a midline surgical incision (1.5–2 cm) was made in the abdominal wall. The mesentery was gently moved out of the abdominal cavity and spread over a pillar for measurements of L_p or over a glass coverslip attached to an animal tray for the confocal microscopy studies. The animal was kept warm on a heating pad, and the upper surface of the mesentery was continuously superfused with warmed (37°C) mammalian Ringer solution. Venular microvessels with brisk blood flow and free of firmly attached leukocytes were selected for the experiments. The diameter of the selected vessels ranged between 40 and 50 μm. Each experiment was carried out on a single microvessel from each animal.

Measurement of hydraulic conductivity. All measurements were based on the modified Landis technique, which measures the volume flux of water across the microvessel wall (8). The assumptions and limitations of the original method and its application to mammalian microvessels have been evaluated in detail elsewhere (13, 21, 26). Briefly, a single venular microvessel was cannulated with a glass micropipette and perfused with albumin-Ringer solution (control) that contained 1% (vol/vol) hamster red blood cells as markers. A hydrostatic pressure (range 40–70 cmH_2O), controlled by a water manometer, was applied through the micropipette to the microvessel lumen to allow the perfusate to flow continuously through the vessel. Video images were recorded from a segment of the perfused microvessel during the experiment. For each measurement, the perfused vessel was briefly occluded downstream with a glass rod for 5–7 s. The initial water flow per unit area of microvessel wall [$(J_v/S)_0$, where J_v is the water flux and S is the unit area of the microvessel wall] was calculated from the velocity of the marker cell after the vessel was occluded, the vessel radius, and the length between the marker cell and the occlusion site. Microvessel L_p was calculated as the slope of the relation between $(J_v/S)_0$ and the pressure difference across the microvessel wall. In each experiment, baseline L_p and the L_p after PAF application were measured in the same vessel, which allowed the PAF-induced change to be compared with its own control. The changes in L_p were expressed as the ratio of PAF-induced L_p to control L_p ($L_{p\ test}/L_{p\ control}$).

Confocal imaging: three-dimensional localization of PAF-induced endothelial gaps in intact microvessels. A Leica TCS SL confocal microscope attached to a single microvessel perfusion rig was used for collecting three-dimensional images from individually perfused microvessels. A stack of confocal images was obtained from each vessel by optical sectioning at successive *x-y* focal planes with a 0.5-μm vertical step (*z*-axis) through the entire vessel depth (diameter) with a Leica ×20 objective (HC Plan APO, numerical aperture 0.7), ×3 electronic zoom, and 1024 × 1024 scan format. The selected pinhole diameter (one airy disk) and the vertical step at *z*-axis were within the effective resolution limitations calibrated for the objective, the wavelength, and the scanning format used in the Leica confocal system. Red fluorescent microspheres (FMs, 100 nm) were used to mark PAF-induced leakage sites on individually perfused microvessels. These FMs contained dyes incorporated into the polymer matrix that produced bright fluorescence with minimal photobleaching and dye leaching. The 100-nm FMs were chosen because they were large enough to be retained within the vessel wall without extravasations into the surrounding tissue (extravasations occurred after perfusion of 30-nm FMs) while small enough to fit into the smallest endothelial gaps (350 × 350 nm), according to reported studies with PAF (2). A helium-neon laser (543 nm, 1.2 mV) at 50% power was used for excitation, and the emission band was 570–630 nm. Identical image acquisition parameters were applied to all of the experiments, which provided comparable images across different experiments. The gain setting maintained the maximum fluorescence at 71–84% of the maximum intensity range for all experiments. The linearity of the system was examined with five solutions of FMs that ranged in concentration from 0.9×10^{11} to 4.4×10^{11} FM/ml, with instrument settings and optical sectioning procedures identical to those used for the perfused vessels. Results show a linear relationship between fluorescence intensity (FI) and FM concentration with a regression coefficient of 0.999.

The control images were acquired after each vessel was perfused with albumin-Ringer solution containing FMs (100 nm at 3.6×10^{11}/ml) for 10 min, followed by albumin-Ringer perfusion alone for 10 min to remove the free FMs from the vessel lumen. To assess the time course of PAF-induced gap formation, FMs were added to the perfusate either at the beginning of PAF perfusion or 30 and 60 min after the start of PAF perfusion. Each FM perfusion was 10 min and was followed by a 10-min washout with PAF alone before images were collected. One stack of images was collected from each vessel at one time point during PAF exposure. To examine the reversibility of FM accumulation, two additional stacks of images were collected from six of the vessels after the FMs had been removed from the perfusate for 30 and 60 min. To investigate whether FM concentration affects PAF-induced FM accumulation, an additional two sets of experiments were conducted with concentrations of 1.8×10^{11} or 7.2×10^{11} FMs/ml. Images presented in Figs. 2–4 and 8 are the projections of either the top half or the bottom half of the *z*-stack images.

Quantification of fluorescent microsphere accumulation in intact microvessels. The FI of the accumulated FMs from a segment of the vessel wall was calculated with the Leica confocal software. The region of interest (ROI) was defined by outlining the vessel boundaries. The total FI of the FMs (i.e., the intensity value of all pixels of the vessel volume) was calculated as area × depth × mean intensity per pixel, where the area is the selected ROI per section and the depth is the total number of images at *z* dimension. Because the FMs were only located at the vessel wall, the FI was quantified as total intensity per square micrometer of vessel wall (FI/*A*). Assuming a cylindrical geometry, surface area of the vessel wall was calculated as $2\pi \times r \times L$, where r is the radius of the microvessel and L is the length of selected ROI from the vessel. PAF-induced changes in total FI per square micrometer of vessel wall were expressed as the ratio of FI/A_{PAF} to $FI/A_{Control}$. Because FM aggregates with adherent leukocytes, the vessel area identified with attached leukocytes was avoided for FI calculations.

To distinguish the changes in FI at the endothelial cell surface from those at endothelial junctions, FI at the endothelial cell surface was also quantified in vessels perfused with FMs under control conditions and after PAF application. Four ROIs were randomly placed on the surface of four endothelial cells (excluding the junctional area) located at the lower half of each vessel wall, and the mean FI/pixel was calculated from all pixels of the cell volume (area of ROI × related image sections). Results are reported as the ratio of endothelial surface mean FI/pixel in PAF-stimulated vessels to that in the control vessels.

Silver staining of endothelial junctions in venular microvessel walls. Venular microvessels were cannulated and perfused with silver nitrate (0.1 g/100 ml) in aqueous solution for 10–20 s and then reperfused with albumin-Ringer perfusate to delineate the endothelial junctions. To prevent blockage of the pipette tip by silver (in the perfusate) and chloride (in the tissue from the superfusate) precipitation during the cannulation process, the tissue was flushed with 5% glucose before the cannulation. Confocal reflectance images (488-nm argon laser excitation) were collected at successive focal planes throughout the entire vessel wall. *z*-Stack images were reconstructed to delineate the endothelial junctions in the vessel wall. Details have been described elsewhere (17).

Electron microscopy. The location of PAF-induced FM accumulation was further examined with electron microscopy. Experimental procedures identical to those described for the confocal studies were conducted before fixation was started. After removal of the perfused FMs from either control or PAF-stimulated microvessels, the upper surface of the mesentery was superfused with a fixative solution of 1% paraformaldehyde, 1.25% glutaraldehyde, and 5% sucrose in 0.1 M phosphate buffer (pH 7.4) for 20 min. After fixation, a small panel of mesentery that contained the perfused microvessel was dissected and placed in the same fixative at 4°C overnight. The specimens were then rinsed in 0.1 M phosphate buffer and permeabilized with 50% ethanol in H_2O. The samples were postfixed in osmium tetroxide (1%), dehydrated in a graded ethanol series, transferred into propylene oxide, and embedded in epon (Ladd LX112). Thin sections were stained with alcoholic uranyl acetate and Reynolds citrate. Photomicrographs (magnification ×32,400) were taken on a JEOL 1220 transmission electron microscope.

Solutions and reagents. Mammalian Ringer solution was used for dissecting mesenteries, superfusing tissue, and preparing the perfusion solutions (21). The composition of the mammalian Ringer solution was (in mM) 132 NaCl, 4.6 KCl, 2 $CaCl_2$, 1.2 $MgSO_4$, 5.5 glucose, 5.0 $NaHCO_3$, 20 *N*-2-hydroxyethylpiperazine-*N*′-2-ethanesulfonic acid (HEPES), and Na-HEPES. The pH of the Ringer solution was maintained at 7.40–7.45 by adjusting the ratio of Na-HEPES to HEPES. All perfusates used for control and test perfusion contained BSA (10 mg/ml).

PAF (1-*O*-alky1-2-acetyl-sn-glycero-3-phosphocholine) (Sigma, St. Louis, MO) was initially dissolved in 95% ethyl alcohol (5 mM) and then further diluted with albumin-Ringer solution to a final concentration of 10 nM. 8-BrcAMP (8-bromo-cAMP sodium salt) was purchased from Sigma. The FMs were purchased from Duke Scientific (Palo Alto, CA). The microspheres are made of polystyrene and are monodisperse polymer microspheres suspended in aqueous solution at a concentration of 1.8×10^{13}/ml. The coefficient of variation for the size of the 100-nm FMs was <10%. The FM suspension was diluted to the desired concentration of FMs with albumin-Ringer solution, and fluorescence imaging confirmed no FM aggregation in the solution. All perfusates that contained the test agent were freshly prepared before each cannulation.

Data analysis and statistics. All values listed in the text are means ± SE, except where noted. Paired *t*-tests were used to analyze the mean values obtained before and after stimulation from the same vessel. Unpaired *t*-tests and one-way ANOVA were used to compare data between groups. A probability value of $P < 0.05$ was considered statistically significant.

RESULTS

Time course of PAF-induced increases in microvessel L_p. To demonstrate the magnitude and time course of PAF-induced permeability increases in intact microvessels, L_p was measured in nine venular microvessels. The mean baseline was $1.3 \pm 0.2 \times 10^{-7}$ cm·s^{-1}·cmH_2O^{-1}. Application of PAF (10 nM) to the perfusate induced a transient increase in L_p in each vessel. Figure 1 shows the time course of PAF-induced increases in L_p pooled from nine vessels. The maximum increase occurred when the vessels were exposed to PAF for 10 min, with a mean peak value at 7.4 ± 1.1 times that of the control. The increased L_p fell to 3.6 ± 0.9 and 2.0 ± 0.3 times the control value at 30 and 60 min, respectively, after the start of PAF perfusion.

Three-dimensional localization of PAF-induced endothelial gaps in intact venular microvessels. FMs were used to perfuse individual microvessels under control conditions or during PAF application. The spatial accumulation of FMs in the vessel wall was three-dimensionally visualized by reconstruction of a stack of confocal images. No increases in FI were detected in the surrounding tissue during the FM perfusion period in either control or PAF-stimulated vessels, indicating that no FMs extravasated across the vessel wall. The accumulation of FMs under control conditions (albumin-Ringer perfusion) was studied in five microvessels. After each vessel was perfused with albumin-Ringer perfusate containing FMs for 10 min, followed by a 10-min washout to remove free FMs from the vessel lumen, the reconstructed confocal images demonstrated a uniform, thin layer of FMs at the surface of the vessel lumen. Figure 2, *left*, shows a representative image projected from the lower half of the image stack from one of the control microvessels. PAF-induced FM accumulation was studied in six microvessels. In contrast to the uniform distribution of FMs under control conditions, perfusion of FMs with PAF for 10 min, followed by a 10-min washout with PAF alone, resulted in a significant amount of preferential accumulation of FMs at vascular walls. Figure 2, *center* and *right*, show representative images from one of the six microvessels, which are the projections of the lower and upper half of the image stack, respectively. As shown by the patterns of endothelial junctions illustrated by the silver nitrite staining (Fig. 3), the FM accumulation showed a near-complete outline of endothelial junctions in PAF-stimulated microvessels. An animated three-dimensional confocal image is provided as an online supplement (Supplemental Video S1).[1]

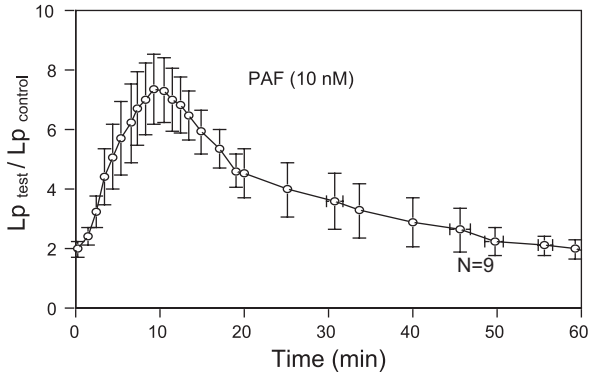

Fig. 1. Time course of platelet-activating factor (PAF)-induced increase in hydraulic conductivity (L_p) pooled from 9 microvessels. Maximum increase in L_p occurred after 10 min of PAF exposure, and L_p fell toward the control value after 60 min of PAF exposure. The first data point was the mean ± SE L_p change relative to control ($L_{p\ test}/L_{p\ control}$) measured at 0.33 min after the start of PAF perfusion.

To investigate the time course of PAF-induced gap formation, two additional groups of experiments were conducted in eight microvessels. In each experiment, FMs were added to the perfusate at 30 ($n = 4$) or 60 ($n = 4$) min after the start of PAF perfusion. The confocal images were collected after a 10-min perfusion of PAF alone. Figure 4 shows three representative images projected from the lower-half image stacks illustrating the spatial accumulation of FMs at 10, 30, and 60 min after the start of PAF perfusion.

Quantification of PAF-induced FM accumulation in intact venular microvessels. To quantify the magnitude of PAF-induced accumulation of FMs, the total FI (area × depth × mean intensity/pixel) per square micrometer of vessel wall was

[1] The online version of this article contains supplemental material.

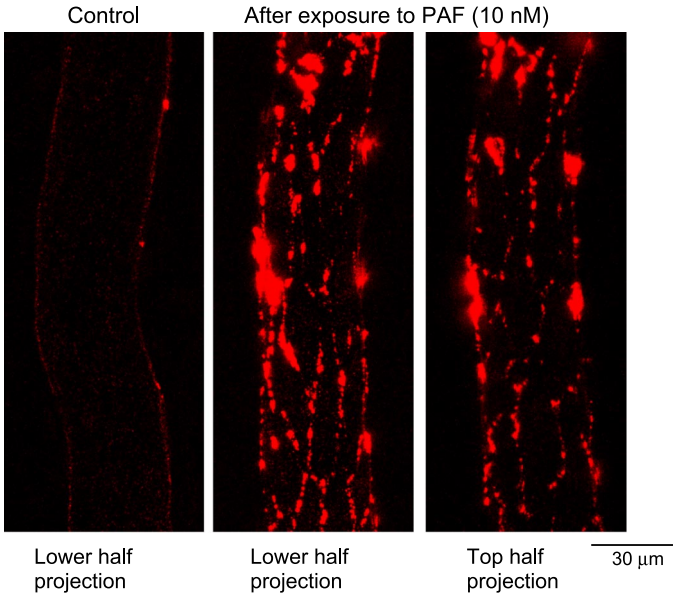

Fig. 2. Confocal images of individually perfused microvessels. *Left*: lower half image stack projection under control conditions. *Center* and *right*: spatial accumulation of fluorescent microspheres (FMs) 10 min after the start of PAF perfusion. Each image is the projection of the lower half or upper half of the *z*-stack images acquired from the same vessel wall.

calculated from each image stack collected from control microvessels and from PAF-stimulated microvessels, where the FMs were added at different times after the start of PAF perfusion. Figure 5*A* shows the time course of the FI calculated from the accumulated FMs and presented as the ratio of FI to *A* in PAF-stimulated vessels relative to that of the control vessels. FI/A was 8.4 ± 1.8 within the first 10 min of PAF plus FM perfusion ($n = 6$) and declined to 5.0 ± 0.6 ($n = 4$) and 1.4 ± 0.2 ($n = 4$) when FMs were added to the perfusate at 30 and 60 min after the start of PAF application, respectively.

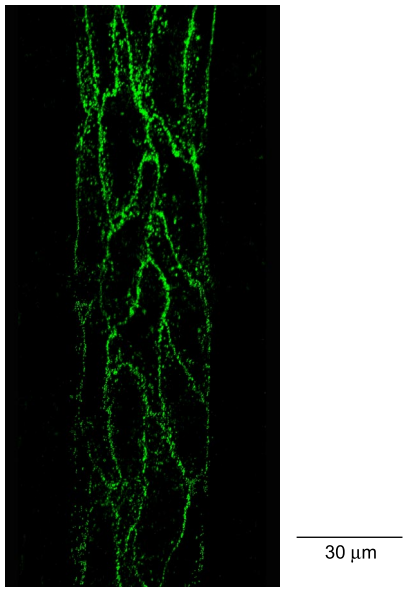

Fig. 3. Confocal image of silver staining: a projection of the lower half of the *z*-stack images obtained from a rat venular mesenteric microvessel, which outlines the pattern of endothelial clefts.

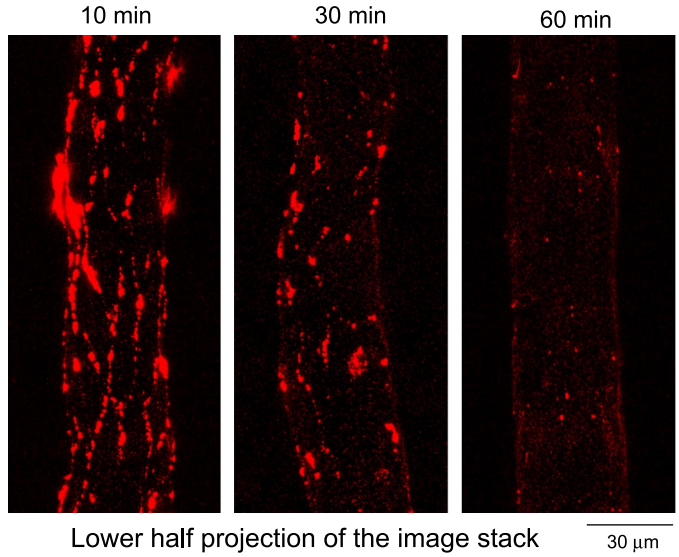

Fig. 4. Representative confocal images from 3 different vessels showing the magnitude differences in the spatial accumulation of FMs when FMs were applied at 10, 30, or 60 min after the start of PAF application.

Figure 5*B* demonstrates that the PAF-induced increases in FI were not caused by the increased FM adherence to the surface of the vessel wall. FI measured on the surface of endothelial cells (excluding the junctional area) showed no significant differences among the four groups of vessels shown in Fig. 5*A*. Figure 5*C* shows the correlation between the magnitude of FM accumulation quantified at three different time points after the start of PAF perfusion and the time course of PAF-induced L_p increases.

Further characterization of FM accumulation in PAF-stimulated microvessels. To test whether the magnitude of PAF-induced accumulation of FMs depends on the concentration of FMs in the perfusate, experiments were conducted on an additional 11 vessels, using either half or double (1.8×10^{11} or 7.2×10^{11} FMs/ml) the concentration of FMs applied in previous experiments (see Fig. 5), while the remaining experimental procedures and image acquisition settings were unchanged. Results showed no significant differences in PAF-induced accumulation of FMs with three different FM concentrations when the FMs were added at the beginning of PAF perfusion for 10 min and the images were collected after a 10-min washout with PAF perfusion alone (Fig. 6). The reversibility of the FM accumulation was examined in the same six microvessels reported in Fig. 5*A* (2nd bar). After the first stack of images was collected after a 10-min washout with PAF alone, each vessel was continuously perfused with PAF and an additional two stacks of images were collected from different regions on each vessel after 30- and 60-min washouts, respectively. Results shown in Fig. 6 indicate that the accumulated FMs could not easily be washed away, even with an extended washout perfusion. Repeated collection of images from the same vessel segments also showed no significant difference in the total intensity of the accumulated FMs, indicating that photobleaching is minimal or negligible under the present experimental conditions.

Electron microscopy. To confirm PAF-induced endothelial gap formation and the junctional accumulation of the FMs at an ultrastructural level, electron microscopy was conducted under

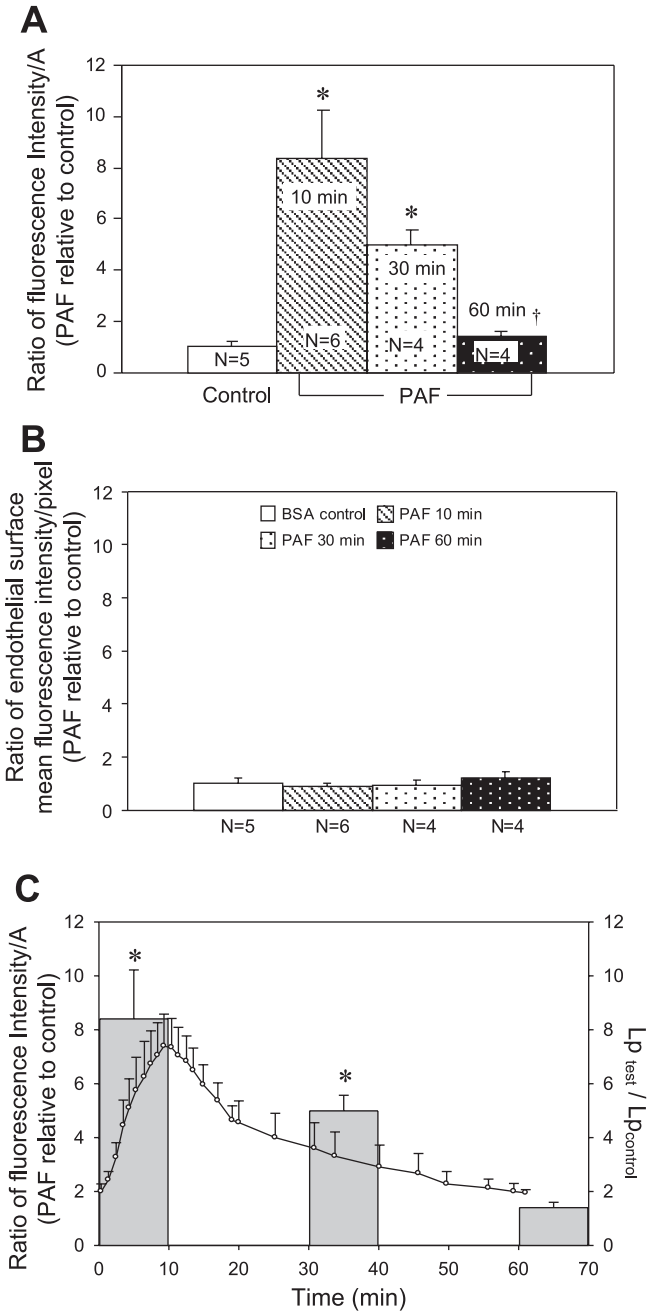

Fig. 5. *A*: quantification of fluorescence intensity (FI) of accumulated FMs on the vessel wall when FMs were applied under control conditions or at 10, 30, and 60 min after the start of PAF perfusion. PAF-induced FM accumulations are expressed as the total FI per μm^2 of vessel wall (FI/*A*) relative to control. *B*: the FI of FMs at the endothelial cell surface (excluding junctional area) was measured in each group of vessels shown in *A*, demonstrating that the PAF-induced increases in FI shown in *A* were not due to increased FM adherence to the endothelial cell surface. *C*: quantitative comparison of the magnitude of PAF-induced accumulation of FMs at 3 different time points with the time course of PAF-induced increases in L_p ($n = 9$). *Significant increase from negative control; †significant decrease from positive control.

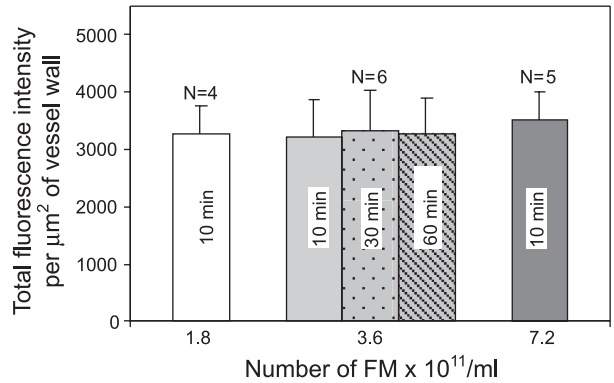

Fig. 6. Summary results of 3 groups of vessels showing that variation of the concentration of FMs in the perfusate from 1.8×10^{11} to 7.2×10^{11} FMs/ml did not affect the magnitude of FM accumulation in PAF-stimulated microvessels. *Center*: bars represent total FI of the FMs quantified from the same group of vessels ($n = 6$) but with different washout periods. All bars represent FI of the accumulated FMs within the first 10 min of PAF exposure.

experimental conditions identical to those used for collecting the confocal images. Figure 7 illustrates a normal endothelial cleft on an albumin-Ringer-perfused vessel (Fig. 7, *top*) and FM accumulation after the vessel was perfused with FMs plus PAF for 10 min, followed by PAF alone during fixation. Although the precise junctional or near-junctional location needs to be confirmed with serial sections, this micrograph confirms the findings of the confocal microscopic studies showing that FMs accumulated at the endothelial junctional areas. The electron micrograph also reveals that each gap was fully occupied by FMs. Therefore, the amount of entrapped FMs enabled them to represent the three-dimensional size of the formed gaps. Additionally, this micrograph illustrates that the basement membrane underneath the open cleft remained intact, which restricted the entrapped FMs from extravasations under the present experimental conditions.

Effect of 8-BrcAMP on PAF-induced endothelial gap formation. We previously demonstrated (19, 20) that perfusion of microvessels with 8-BrcAMP prevented agonist-induced increases in microvessel L_p. Experiments were conducted in six microvessels to evaluate whether the inhibitory effect of 8-BrcAMP on microvessel permeability was due to the inhibition of endothelial gap formation. In four of the microvessels, confocal images were collected after perfusion with albumin-

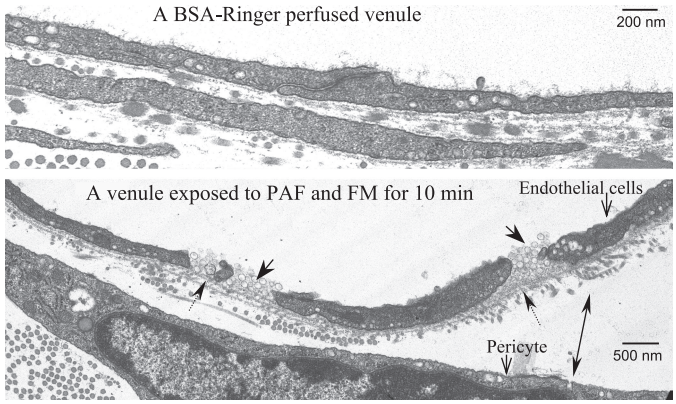

Fig. 7. Ultrastructural examination of endothelial junctions of microvessels perfused with albumin-Ringer solution (control, *top*) or PAF + FMs (*bottom*). *Top*: an intact endothelial junction from a microvessel perfused with albumin-Ringer solution. *Bottom*: PAF-induced endothelial gap formation and junctional accumulation of FMs. FM accumulation is indicated by single arrows with solid line. The arrow with a dotted line indicates the intact basement membrane underneath the gaps. The double arrow indicates the increased space between an endothelial cell and a pericyte.

Ringer perfusate containing 8-BrcAMP (2 mM) for 20 min followed by 8-BrcAMP, PAF (10 nM), and FM perfusion for 10 min and a 10-min washout with PAF alone. The application of 8-BrcAMP significantly inhibited PAF-induced FM accumulation. Figure 8*A*, *left*, shows one of the representative images. In another two microvessels, we examined whether the inhibitory effect of 8-BrcAMP on PAF-induced gap formation can be restored after 8-BrcAMP is washed out. The perfusions of 8-BrcAMP and 8-BrcAMP plus PAF were the same as those used for the other four vessels, except that the FMs were not added during the first PAF addition. Each vessel was then perfused with albumin-Ringer solution for 30 min to wash out 8-BrcAMP and PAF before PAF and FM perfusion for 10 min. The images collected after 10-min FM washout with PAF alone demonstrate a partial restoration of PAF-induced endothelial gap formation (Fig. 8*A*, *right*). The ratio of the mean FI/*A* in 8-BrcAMP- and PAF-perfused vessels to that of the control was 0.7 ± 0.2. After removal of 8-BrcAMP and PAF, the mean FI/*A* of the second PAF administration was 2.6 ± 0.1 times the control value and 3.7 ± 0.1 times the value in vessels perfused with 8-BrcAMP and PAF. The changes in FI/*A* relative to control values are summarized in Fig. 8*B*.

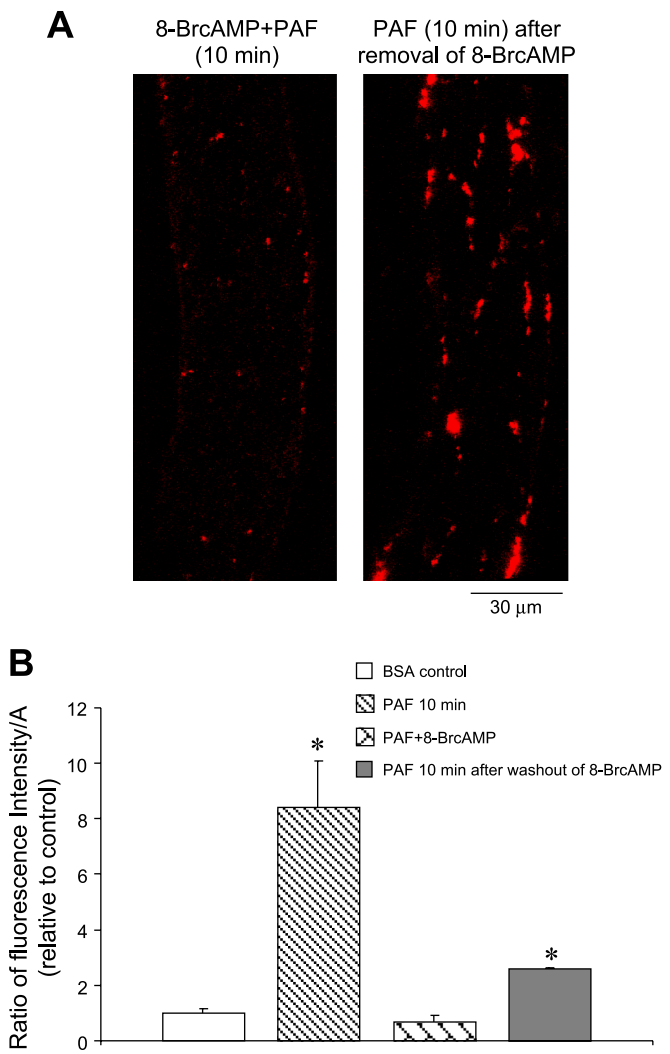

Fig. 8. Effect of 8-bromo-cAMP (8-BrcAMP) on PAF-induced gap formation. *A*: preperfusing a vessel with 8-BrcAMP (2 mM) significantly inhibited PAF-induced FM accumulation at endothelial junctions (*left*), and the junctional FM accumulation was partially restored when PAF was applied the 2nd time after 8-BrcAMP and PAF were washed out with albumin-Ringer perfusion for 30 min (*right*). Each image is the lower half projection of the image stack. *B*: comparisons of total FI per μm^2 of vessel wall (FI/*A*) in vessels under control conditions ($n = 5$), within 10 min of PAF application in the absence ($n = 6$) or presence of 8-BrcAMP ($n = 4$), and after 2nd application of PAF after removal of 8-BrcAMP ($n = 2$). *Significant increase from negative control.

DISCUSSION

This study presents a new experimental approach that allows three-dimensional visualization and quantification of agonist-induced gap formation on intact microvessels using combined single vessel perfusion technique with fluorescence confocal microscopy. One of the unique features of this method is that the entrapped FMs at open endothelial clefts represented the maximum dimensions of the gaps during the FM perfusion period, thus allowing a quantitative evaluation of the magnitude of the endothelial gaps formed on the vascular wall. By adding FMs to the perfusate at different times after the start of agonist application, this technique also allowed a dynamic assessment of gap status on stimulated microvessels. More importantly, the experimental procedures used to illustrate endothelial gaps were identical to those used to measure permeability coefficients, endothelial $[Ca^{2+}]_i$, and NO production in individually perfused microvessels (42). Therefore, quantitative comparisons can be made between the magnitude of the formed endothelial gaps and functional measurements of the permeability properties of the vascular walls, thereby allowing the identification of transport pathways and cellular mechanisms responsible for increased permeability. The technique also provides a means for spatial correlation between the cellular signaling and endothelial gap formation in stimulated vascular walls. The temporal and spatial visualization of endothelial gaps is a complement to the quantitative measurements of permeability coefficients in individually perfused microvessels.

Using this newly developed technique, our study demonstrated a close relationship between the dynamic changes in the magnitude of the formed endothelial gaps and the transient increase in microvessel L_p. Electron microscopy conducted on vessels that experienced the same experimental procedures revealed that FMs in PAF-stimulated microvessels fully occupied the open clefts and were retained by the intact basement membrane, thus providing ultrastructural evidence that the amount of accumulated FMs enables them to represent the dimensions of the open endothelial clefts under defined experimental conditions.

Unique features of using FMs and confocal microscopy to illustrate temporal and spatial formation of endothelial gaps in individually perfused intact microvessels. In individually perfused microvessels, changes in permeability properties of the microvascular walls are usually measured in the absence of blood by either L_p or solute permeability coefficient (13, 25, 26, 41). Even though the perfused vessel may not be completely equivalent to the vessel in its "resting state" because of the minor surgery procedure and protein composition differences in the perfusate, measurements from individually perfused vessels usually provide the most quantitative assessments of the transport function of the vascular walls in vivo because

of their known driving force, surface area for exchange, and precisely controlled perfusion pressure. However, the reported values are the total net fluxes divided by the surface area of the vessel wall. They cannot characterize the spatial heterogeneity of the leakage sites or identify transport pathways.

For decades, gap formation between endothelial cells has been indicated as the main transport pathway responsible for increased permeability to fluid and macromolecules during inflammation (8–10, 16, 28, 36, 37). The documented evidence was mainly obtained from ultrastructural studies using combined carbon tracer and electron microscopy, which provided quantitative comparisons among transport functions, the dimensions of the formed gaps, and other ultrastructural changes (8). However, because of the limited region of each micrograph, the work was very time consuming, and it was almost impossible to provide a general picture of the structural changes that occurred along the entire vessel segment, for which the permeability coefficients are usually measured. Therefore, mathematical modeling was usually used to estimate the number and size of the formed pores under different permeability states (7, 11, 27, 28, 32, 34–36). Other commonly used methods to assess the magnitude of the permeability increase and the size of the formed gaps were counting the number of large leaky sites at a defined area in a vascular bed with systemically injected fluorescent markers (24, 31, 32, 37). These studies were usually conducted in the presence of blood flow, representing a normal pathophysiological reaction, and significantly contributed to the understanding of the transport process during inflammation but had limited capacity for dissecting the roles of individual components and investigating detailed cellular mechanisms. The two-dimensional analysis of three-dimensional leakage sites, the uncertainties of hemodynamic factors, and the unknown surface area for transport are also concerns. A recent study by Baffert et al. (3) established a confocal microscopic approach to identify the endothelial gaps in mice tracheal venules via sequential injections of agonist and FMs into the venular circulation, followed by intravascular tissue fixation. The present study extended that technique and directly applied the agonist and FMs to individually perfused microvessels in the absence of blood flow. This approach has many unique advantages over existing methods. Because FMs easily attach to adherent leukocytes, the absence of blood flow prevented or minimized aggregation of FMs with any blood cells adhered to the vessel wall. Our results (Fig. 5*B*) also showed that there was no increased FM adherence to the endothelial cell surface after PAF application. Thus, under the present experimental conditions after the free FMs from the vessel lumen were washed away, the magnitude of the FM accumulation more accurately represented the extent of endothelial gap formation. Another advantage is that each perfused vessel was exposed to precise concentrations of agonist and FMs under well-controlled perfusion pressure and exposure duration, which avoided the uncertainties of hemodynamic effects on agonist and tracer distribution and enabled rigorous comparisons across experiments. Additionally, the perfused vessels had translucent vessel lumens that permitted good laser penetration, and the perfusion pressure maintained the original vessel geometry, which allowed optical sectioning and image acquisition through the entire vessel wall without the need for fixation. The reconstructed confocal images provide a three-dimensional view of the spatial accumulation of FMs in an entire segment of a perfused microvessel. These results have not been achieved previously. By adding FMs to the perfusate at different time points after the start of PAF perfusion, this method also allows a dynamic evaluation of gap formation.

Although gap formation has been reported with a variety of agents, it remains to be determined whether all permeability increases are the result of endothelial gap formation (12, 35). With parallel permeability measurements, this method not only allows investigation of the transport pathways of a specific mediator-induced permeability increase but also enables us to identify the mechanisms of certain reagents that prevent permeability increases. The study of the effect of 8-BrcAMP on PAF-induced gap formation provided one example of these utilities. Previous studies demonstrated that β_2 adrenergic receptor agonists or cAMP enhancing agents, such as 8-BrcAMP, prevent inflammatory mediator-induced permeability increases (1, 6, 19–21). Our present study demonstrated that 8-BrcAMP inhibited PAF-induced gap formation, which may explain the inhibitory action of 8-BrcAMP on microvessel permeability. It has also been reported that some anti-inflammatory agents inhibited plasma leakage without blocking endothelial gap formation, indicating the existence of gap-independent mechanisms regulating microvessel permeability (4). This method may serve as an efficient tool for distinguishing gap-dependent from gap-independent mechanisms of any pro- or anti-inflammatory agents.

PAF-induced junctional accumulation of FMs serves as quantitative measure of magnitude of endothelial gaps in intact microvessels. This technique was developed to provide a three-dimensional view of leakage sites on intact microvessels and is an advancement over existing methodologies. One question that remains is whether or not FM accumulation at leakage sites can be used to quantify the magnitude of the endothelial gaps. The unique physical properties of the FMs make them excellent tracers for quantitative fluorescence microscopy. First, the fluorescent dye is incorporated into the polymer matrix of the microspheres, which has minimal photobleaching and dye leaching. Second, FMs have uniform dimensions and do not aggregate in aqueous solutions. They are also available in a variety of sizes, which enables the investigation of different molecular sieving properties of each barrier on the microvessel walls. The reported size of PAF-induced endothelial gaps ranges between 350 × 350 nm and 1,000 × 600 nm (2). The use of 100-nm FMs might be optimal for PAF- or other inflammatory mediator-induced gaps, because they are large enough to be retained within the vessel wall while being small enough to fit into the smallest endothelial gaps at peak responses. However, for more subtle changes or smaller-sized gaps, smaller FMs might provide a higher sensitivity, as long as they can be retained by the basement membrane. Additionally, FMs can be identified by electron microscopy, which enables ultrastructural registration of FMs that appear in the fluorescence images.

In the present study, the results of fluorescence microscopy demonstrated that the 100-nm FMs were not extravasated from either control or PAF-stimulated microvessels and PAF-induced FM accumulation at the vessel wall was mainly at endothelial junctions. This correlated with the pattern of silver staining from confocal images and was confirmed ultrastructurally by electron microscopy. Results of the present study also revealed that the amount of PAF-induced accumulation of

FMs was not significantly different when the FM concentration was varied from one-half to twofold the initial concentration (Fig. 6) and there was no increased FM adhesion at endothelial cell surface after PAF application (Fig. 5*B*). These results suggest that as long as the amount of FMs in the perfusate is sufficient to fill the open clefts, excess FMs are removed by the washout perfusion and do not affect the magnitude of the FM accumulation. Therefore, the amount of accumulated FMs is dependent on the dimensions of the intercellular gaps and independent of the concentration of FMs in the perfusate, at least within the concentration range tested in the present study. Extending the duration of the washout perfusion from 10 min to 30 and 60 min also did not significantly affect the FI of the accumulated FMs. These findings suggest that the FMs entrapped at open clefts were not easily washed away and that the presence of the FMs actually locked the gap at a particular size and prevented its closure.

Together, these results indicate that in PAF-stimulated microvessels the total FI of the accumulated FMs from the entire *z*-stack image enabled them to represent the total volume of the formed gaps on that segment of the vessel wall. However, overestimation or underestimation may occur if the FMs attach to any adherent blood cells or leak into the endothelial/pericyte space or surrounding tissues.

Direct comparisons of magnitude of gap formation with magnitude of permeability increase. It is well known that most inflammatory mediators, such as histamine, bradykinin, substance P, and PAF, induce transient increases in microvessel permeability, i.e., the increased permeability recovers even in the continuous presence of the agonist (2, 5, 18, 22, 27, 38, 39). Although the mechanisms responsible for the recovery phase remain unidentified, the endothelial gaps have been considered the principal sites for the onset of plasma leakage or the hydraulic pathway through the vascular walls (8, 12, 14, 24, 28, 30, 32, 36, 37). Recently, different approaches have been developed by McDonald and colleagues (5, 29) to demonstrate the presence of endothelial gaps and correlative vessel leakage on stimulated microvasculature of rat or mouse trachea after fixation. In substance P-stimulated venules from the rat trachea a transient time course for the formation and closure of endothelial gaps was reported, but it was found that the amount of extravasated Monastral blue was decreased before gap closure. This discrepancy was explained by the possibility of a decrease in the driving force for the convective movement of the tracer (29). In our present study, considering the potential interference of the entrapped FMs at endothelial gaps with the subsequent solute and fluid transport, the measurements of L_p and FM accumulation were examined in different groups of vessels, but with identical experimental preparations. Results showed that both the mean peak L_p and the maximum FM accumulation occurred within 10 min of the start of PAF perfusion. Up to 30 min after the start of PAF exposure, L_p and FM accumulation declined at a similar magnitude toward the control level as indicated in Fig. 5*C*. A slight difference occurred after 60 min of PAF perfusion, in that the FM accumulation was not significantly different from the control group ($P = 0.07$) but L_p remained slightly higher than the control value ($P < 0.05$). This can be attributed to a reduction in the endothelial gap sizes that restricted FM filtration at 100 nm but remained sufficient for a small degree of elevated L_p. Although gap opening and closing has been reported in microvessels exposed to inflammatory agents, such as bradykinin or substance P, the present results are the first to demonstrate that opening and closing of endothelial gaps also occurred with a PAF-induced increase in permeability.

The correlation between changes in the magnitude of FM accumulation and changes in the magnitude of the L_p increase indicated that PAF-induced endothelial gap formation and subsequent closure play a dominant role in determining the magnitude of the L_p increase. However, this finding does not conclude that the endothelial cells are the sole barrier for fluid and solute transport. Some previous studies revealed that if fluid filtration is proportional to the third power of the width of the cleft (Poiseuille's law for a parallel-walled slit), the change in L_p should be at a much larger magnitude than what has previously been reported. The calculation was based on the assumption that 1 out of 5 or 6 intercellular junctions per circumference becomes a gap 10 times wider than a normal cleft at its widest point (8). Confocal images of the present study actually indicated a higher percentage of open clefts in PAF-stimulated microvessels than the predicted ratio of 1 to 5 or 6, but the mean increase in the peak L_p was only 7.4 times the control value. These results further support the existence of multiple barriers for water and solute transport in the venular microvessel wall. Our results indicated that the open endothelial clefts are essential in determining the fluid and solute transport, assuming that the other vascular structures remained relatively intact. In addition to the endothelial barrier, other structures in the vessel wall, such as fiber matrix, basement membrane, and pericyte layer, may also provide significant resistance for fluid and solute transport (8, 9, 12, 32). The electron micrographs (Fig. 7) demonstrate an area with increased space between the endothelial cells and pericytes, an indication of accumulated fluid in that space, which must be the result of additional resistance provided by the pericyte layer.

Currently, the mechanisms that cause the formation and closure of gaps remain poorly understood. Most in vitro studies have indicated that gap formation is regulated by the balance of competing contractile and adhesive forces that modulate cell shape (15). A variety of signaling cascades have been proposed to regulate these mechanisms (15, 31), but most studies were conducted in vitro and have not been validated in vivo (31, 32). Previous work from this laboratory (42) demonstrated that microvessels exposed to PAF transiently increased endothelial $[Ca^{2+}]_i$ and that calcium-dependent increased NO production via endothelial nitric oxide synthase activation is necessary for increased L_p. Whether these signaling pathways directly contribute to the formation of endothelial gaps remains unknown. The experimental approach presented here provides an efficient tool to allow a direct correlation between gap formation and cellular signaling in intact microvessels.

Limitations of the method. As stated above, the combination of confocal microscopy and FM to visualize and quantify the formed endothelial gaps is a very useful tool for investigating the cellular mechanisms of increased microvessel permeability in individually perfused microvessels. However, we understand that the perfused microvessels in the absence of blood are different to certain degrees from their native states. It should not be overlooked that, in the presence of blood, the mediators released from the activated cells and leukocyte/platelet/endothelium interactions are essential for endothelial cell activation

and gap formation during inflammation. Because FMs have the tendency to attach to the adherent leukocytes, especially leukocytes often preferentially adhere at endothelial junctions (40); thus the FM accumulation at vascular walls, if injected into the bloodstream, may not accurately represent leukocyte/platelet/endothelium interaction-induced endothelial gap formation in the whole vascular beds.

GRANTS

This study was supported by National Heart, Lung, and Blood Institute Grants HL-56237 and HL-084338.

The findings and conclusions in this report are those of the author(s) and do not necessarily represent the views of the National Institute for Occupational Safety and Health.

REFERENCES

1. **Adamson RH, Liu B, Fry GN, Rubin LL, Curry FE.** Microvascular permeability and number of tight junctions are modulated by cAMP. *Am J Physiol Heart Circ Physiol* 274: H1885–H1894, 1998.
2. **Adamson RH, Zeng M, Adamson GN, Lenz JF, Curry FE.** PAF- and bradykinin-induced hyperpermeability of rat venules is independent of actin-myosin contraction. *Am J Physiol Heart Circ Physiol* 285: H406–H417, 2003.
3. **Baffert F, Le T, Thurston G, McDonald DM.** Angiopoietin-1 decreases plasma leakage by reducing number and size of endothelial gaps in venules. *Am J Physiol Heart Circ Physiol* 290: H107–H118, 2006.
4. **Baluk P, Fine NW, Thomas HA, Wei ET, McDonald DM.** Anti-inflammatory mystixin peptides inhibit plasma leakage without blocking endothelial gap formation. *J Pharmacol Exp Ther* 284: 693–699, 1998.
5. **Baluk P, Hirata A, Thurston G, Fujiwara T, Neal CR, Michel CC, McDonald DM.** Endothelial gaps: time course of formation and closure in inflamed venules of rats. *Am J Physiol Lung Cell Mol Physiol* 272: L155–L170, 1997.
6. **Baluk P, McDonald DM.** The β_2-adrenergic receptor agonist formoterol reduces microvascular leakage by inhibiting endothelial gap formation. *Am J Physiol Lung Cell Mol Physiol* 266: L461–L468, 1994.
7. **Baxter LT, Jain RK, Svensjo E.** Vascular permeability and interstitial diffusion of macromolecules in the hamster cheek pouch: effects of vasoactive drugs. *Microvasc Res* 34: 336–348, 1987.
8. **Clough G, Michel CC.** Quantitative comparisons of hydraulic permeability and endothelial intercellular cleft dimensions in single frog capillaries. *J Physiol* 405: 563–576, 1988.
9. **Clough G, Michel CC, Phillips ME.** Inflammatory changes in permeability and ultrastructure of single vessels in the frog mesenteric microcirculation. *J Physiol* 395: 99–114, 1988.
10. **Cotran RS, Majno G.** A light and electron microscopic analysis of vascular injury. *Ann NY Acad Sci* 116: 750–764, 1964.
11. **Curry FE.** Determinants of capillary permeability: a review of mechanisms based on single capillary studies in the frog. *Circ Res* 59: 367–380, 1986.
12. **Curry FE, Adamson RH.** Transendothelial pathways in venular microvessels exposed to agents which increase permeability: the gaps in our knowledge. *Microcirculation* 6: 3–5, 1999.
13. **Curry PE, Huxley VH, Sarelius IH.** Techniques in microcirculation: measurement of permeability, pressure and flow. In: *Cardiovascular Physiology. Techniques in the Life Sciences*. New York: Elsevier, 1983.
14. **Feng D, Nagy JA, Pyne K, Hammel I, Dvorak HF, Dvorak AM.** Pathways of macromolecular extravasation across microvascular endothelium in response to VPF/VEGF and other vasoactive mediators. *Microcirculation* 6: 23–44, 1999.
15. **Garcia JG, Davis HW, Patterson CE.** Regulation of endothelial cell gap formation and barrier dysfunction: role of myosin light chain phosphorylation. *J Cell Physiol* 163: 510–522, 1995.
16. **Granger HJ, Schelling ME, Lewis RE, Zawieja DC, Meininger CJ.** Physiology and pathobiology of the microcirculation. *Am J Otolaryngol* 9: 264–277, 1988.
17. **He P, Adamson RH.** Visualization of endothelial clefts and nuclei in living microvessels with combined reflectance and fluorescence confocal microscopy. *Microcirculation* 2: 267–276, 1995.
18. **He P, Curry FE.** Depolarization modulates endothelial cell calcium influx and microvessel permeability. *Am J Physiol Heart Circ Physiol* 261: H1246–H1254, 1991.
19. **He P, Curry FE.** Differential actions of cAMP on endothelial $[Ca^{2+}]_i$ and permeability in microvessels exposed to ATP. *Am J Physiol Heart Circ Physiol* 265: H1019–H1023, 1993.
20. **He P, Zeng M, Curry FE.** Dominant role of cAMP in regulation of microvessel permeability. *Am J Physiol Heart Circ Physiol* 278: H1124–H1133, 2000.
21. **He P, Zhang H, Zhu L, Jiang Y, Zhou X.** Leukocyte-platelet aggregate adhesion and vascular permeability in intact microvessels: role of activated endothelial cells. *Am J Physiol Heart Circ Physiol* 291: H591–H599, 2006.
22. **He P, Zhang X, Curry FE.** Ca^{2+} entry through conductive pathway modulates receptor-mediated increase in microvessel permeability. *Am J Physiol Heart Circ Physiol* 271: H2377–H2387, 1996.
23. **Hirata A, Baluk P, Fujiwara T, McDonald DM.** Location of focal silver staining at endothelial gaps in inflamed venules examined by scanning electron microscopy. *Am J Physiol Lung Cell Mol Physiol* 269: L403–L418, 1995.
24. **Hulstrom D, Svensjo E.** Intravital and electron microscopic study of bradykinin-induced vascular permeability changes using FITC-dextran as a tracer. *J Pathol* 129: 125–133, 1979.
25. **Huxley VH, Curry FE, Adamson RH.** Quantitative fluorescence microscopy on single capillaries: alpha-lactalbumin transport. *Am J Physiol Heart Circ Physiol* 252: H188–H197, 1987.
26. **Kendall S, Michel CC.** The measurement of permeability in single rat venules using the red cell microperfusion technique. *Exp Physiol* 80: 359–372, 1995.
27. **Korthuis RJ, Wang CY, Spielman WS.** Transient effects of histamine on the capillary filtration coefficient. *Microvasc Res* 28: 322–344, 1984.
28. **Majno G, Palade GE.** Studies on inflammation. 1. The effect of histamine and serotonin on vascular permeability: an electron microscopic study. *J Biophys Biochem Cytol* 11: 571–605, 1961.
29. **McDonald DM.** Endothelial gaps and permeability of venules in rat tracheas exposed to inflammatory stimuli. *Am J Physiol Lung Cell Mol Physiol* 266: L61–L83, 1994.
30. **McDonald DM, Thurston G, Baluk P.** Endothelial gaps as sites for plasma leakage in inflammation. *Microcirculation* 6: 7–22, 1999.
31. **Mehta D, Malik AB.** Signaling mechanisms regulating endothelial permeability. *Physiol Rev* 86: 279–367, 2006.
32. **Michel CC, Curry FE.** Microvascular permeability. *Physiol Rev* 79: 703–761, 1999.
33. **Michel CC, Neal CR.** Openings through endothelial cells associated with increased microvascular permeability. *Microcirculation* 6: 45–54, 1999.
34. **Pappenheimer JR, Renkin EM, Borrero LM.** Filtration, diffusion and molecular sieving through peripheral capillary membranes; a contribution to the pore theory of capillary permeability. *Am J Physiol* 167: 13–46, 1951.
35. **Renkin EM.** Relation of capillary morphology to transport of fluid and large molecules: a review. *Acta Physiol Scand Suppl* 463: 81–91, 1979.
36. **Rippe B, Haraldsson B.** Transport of macromolecules across microvascular walls: the two-pore theory. *Physiol Rev* 74: 163–219, 1994.
37. **Svensjö E, Roempke K.** Microvascular aspects of oedema formation and its inhibition by b2-receptor stimulants and some other anti-inflammatory drugs. *In Progress in Microvascular Research II*, edited by Courtice FC, Garlick DC, Perry MA. Sydney, Australia: University of New South Wales, 1984, p. 449–463.
38. **Wu NZ, Baldwin AL.** Possible mechanism(s) for permeability recovery of venules during histamine application. *Microvasc Res* 44: 334–352, 1992.
39. **Wu NZ, Baldwin AL.** Transient venular permeability increase and endothelial gap formation induced by histamine. *Am J Physiol Heart Circ Physiol* 262: H1238–H1247, 1992.
40. **Zeng M, Zhang H, Lowell C, He P.** Tumor necrosis factor-α-induced leukocyte adhesion and microvessel permeability. *Am J Physiol Heart Circ Physiol* 283: H2420–H2430, 2002.
41. **Zhu L, Castranova V, He P.** fMLP-stimulated neutrophils increase endothelial $[Ca^{2+}]_i$ and microvessel permeability in the absence of adhesion: role of reactive oxygen species. *Am J Physiol Heart Circ Physiol* 288: H1331–H1338, 2005.
42. **Zhu L, He P.** Platelet-activating factor increases endothelial $[Ca^{2+}]_i$ and NO production in individually perfused intact microvessels. *Am J Physiol Heart Circ Physiol* 288: H2869–H2877, 2005.